Multiporphyrinic Rotaxanes: Control of Intramolecular Electron Transfer Rate by Steering the Mutual Arrangement of the Chromophores

Myriam Linke,[†] Jean-Claude Chambron,*[,†] Valérie Heitz,[†] Jean-Pierre Sauvage,*[,†] Susana Encinas,[‡] Francesco Barigelletti,[‡] and Lucia Flamigni*[,‡]

Contribution from the Laboratoire de Chimie Organo-Minérale, Institut Le Bel, Université Louis-Pasteur, 4, rue Blaise Pascal, 67070 Strasbourg Cedex, France and the Istituto FRAE-CNR, Via P. Gobetti, 101, 40129 Bologna, Italy

Received June 6, 2000

Abstract: A [2]-rotaxane $\mathbf{Zn_2}-\mathbf{Au}^+$ made from a dumbbell component ended by Zn(II) porphyrin stoppers and a ring component incorporating a Au(III) porphyrin has been assembled in 13% yield using the transition metal templating route. ^{1}H NMR studies show that its conformation in solution is very different from those of its complexes with Cu^+, Ag^+, and Li^+. In particular, removal of the templating metal resulted in a changeover of the molecule, the threaded macrocycle undergoing a pirouetting motion placing the Au(III) porphyrin in the cleft formed by the two Zn(II) porphyrin stoppers. At room temperature, the changeover could be either complete or partial, depending on the solvent used. Photoinduced electron transfer from one of the Zn(II) porphyrins to the Au(III) porphyrin of the macrocycle was evidenced in the case of the free rotaxane and its Cu(I) complex, $\mathbf{Zn_2Cu}^+\mathbf{Au}^+$. In the former case, the photoinduced electron transfer process could be clearly resolved for an extended conformation that is characterized by the Zn(II) porphyrins pointing far from the Au(III) porphyrin electron acceptor, and accounting for 30% of the total in acetonitrile at room temperature. In both $\mathbf{Zn_2Cu}^+$-$\mathbf{Au}^+$ and $\mathbf{Zn_2}-\mathbf{Au}^+$ rotaxanes, the charge-separated state, in which the Zn(II) porphyrin is a cation radical and the Au(III) porphyrin a neutral radical, was generated at a rate of 5×10^9 s^{-1} and disappeared at a rate of 2×10^8 s^{-1}. In the case of $\mathbf{Zn_2Cu}^+\mathbf{Au}^+$, the primary step is very likely energy transfer from the Zn(II) porphyrin singlet excited state to the MLCT state of the central Cu(I) complex, followed by an electron transfer from the excited Cu(I) unit to the Au(III) porphyrin and a successive charge shift from the Zn(II) porphyrin to the oxidized Cu(II) complex. [2]-rotaxane $\mathbf{Zn_2}-\mathbf{Au}^+$, in which no bond pathway can be identified between the donor and the acceptor, is a typical case of electron transfer involving molecular fragments connected by mechanical bonds.

Introduction.

The study of electron transfer (ET) and/or energy transfer (EN) between porphyrins or analogues is of high biological relevance.[1] Examples of natural ET porphyrins are the cytochromes of the mitochondrial respiratory chain, which convey electrons to the terminal cytochrome oxidase complex, and chlorophylls, which, as dimeric structures known as P680 and under light activation, pump electrons from the oxygen-evolving complex (OEC) of the photosystem II (PS II) of green plants.[2a] As far as natural EN is concerned, the so-called light-harvesting complexes massively rely on porphyrinic chromophores for collection and transduction of light energy to the reaction center (RC).[2b,c]

Our groups have been interested for several years in mimicking the function of the special pair (SP)/bacteriopheophytin (BPh) dyad of the bacterial photosynthetic reaction center, the structure of which had been solved by X-ray crystallography.[2d,e] SP, as a bacteriochlorophyll dimer, is the primary electron donor in its excited state, and BPh is the secondary electron acceptor, being established at least at room temperature, that the primary electron acceptor is a bacteriochlorophyll (BCh) cofactor located between SP and BPh.[3] We used Zn(II) or free-base porphyrins as SP mimics and introduced Au(III) porphyrins as functional models of BPh.[4] We developed and studied both linear triadic arrays assembled around Ru(II) and Ir(III) terpyridine complexes[5] and oblique systems connected by a 1,10-phenanthroline

[†] Université Louis-Pasteur.

[‡] Istituto FRAE-CNR.

(1) (a) McLendon, G.; Hake, R. *Chem. Rev.* **1992**, *92*, 481−490. (b) Wasielewski, M. R. *Chem. Rev.* **1992**, *92*, 435−461. (c) Gust, D.; Moore, A. T.; Moore, A. L. *Acc. Chem. Res.* **1993**, *26*, 198−205. (d) Kurreck, H.; Huber, M. *Angew. Chem., Int. Ed. Engl.* **1995**, *34*, 849−866. (e) Harriman, A.; Sauvage, J.-P. *Chem. Soc. Rev.* **1996**, 41−48.

(2) (a) Rawn, J. D. *Biochemistry*; Neil Patterson Publishers: Burlington, North Carolina, 1989. (b) Kühlbrandt, W.; Wang, D. N.; Fujiyoshi, Y. *Nature* **1994**, *367*, 614−621. (c) McDermott, G.; Prince, S. M.; Freer, A. A.; Hawthornthwaite-Lawless, A. M.; Papiz, M. Z.; Cogdell, R. J.; Isaacs, N. W. *Nature* **1995**, *374*, 517−521. (d) Deisenhofer, J.; Michel, H. *Angew. Chem., Int. Ed. Engl.* **1989**, *28*, 829−847. (e) Huber, R. *Angew. Chem., Int. Ed. Engl.* **1989**, *28*, 848−869.

(3) (a) Scherer, P. O. J.; Fischer, S. F. *Chem. Phys. Lett.* **1987**, *141*, 179−185. (b) Warshel, A.; Creighton, S.; Parson, W. W. *J. Phys. Chem.* **1988**, *92*, 2696−2701. (c) Dressler, K.; Umlauf, E.; Schmidt, S.; Hamm, P.; Zinth, W.; Buchanan, S.; Michel, H. *Chem. Phys. Lett.* **1991**, *183*, 270−276. (d) Chan, C.-K.; DiMagno, T. J.; Chen, L. X.-Q.; Norris, J. R.; Fleming, G. R. *Proc. Natl. Acad. Sci. U.S.A.* **1991**, *88*, 11202−11206. (e) Arlt, T.; Schmidt, S.; Kaiser, W.; Lauterwasser, C.; Meyer, M.; Scheer, H.; Zinth, W. *Proc. Natl. Acad. Sci. U.S.A.* **1991**, *88*, 11757−11761.

(4) (a) Chardon-Noblat, S.; Sauvage, J.-P.; Mathis, P. *Angew. Chem., Int. Ed. Engl.* **1989**, *28*, 593−595. (b) Heitz, V.; Chardon-Noblat, S.; Sauvage, J.-P. *Tetrahedron Lett.* **1991**, *32*, 197−198. (c) Brun, A. M.; Harriman, A.; Heitz, V.; Sauvage, J.-P. *J. Am. Chem. Soc.* **1991**, *113*, 8647−8663. (d) Harriman, A.; Heitz, V.; Ebersole, M.; van Willigen, H. *J. Phys. Chem.* **1994**, *98*, 4982−4989.

10.1021/ja002018f CCC: $19.00
Published on Web 12/06/2000

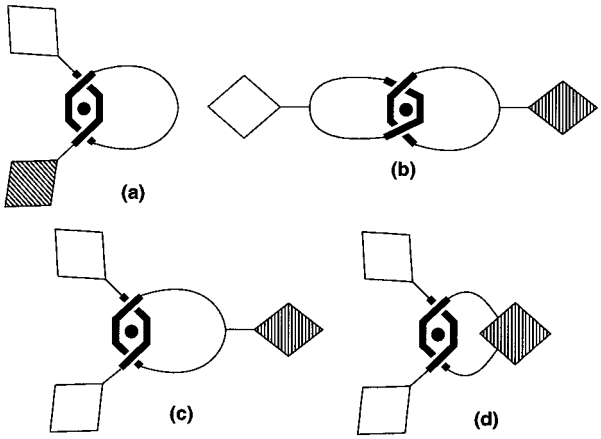

Figure 1. Schematic representation of metal-complexed [2]-rotaxanes (a, c, and d) and [2]-catenane (b). The thick lines represent chelating fragments, the black disk is a metal cation, the empty diamonds are Zn(II) porphyrins, and the hatched diamonds are Au(III) porphyrins.

spacer.[4,6,7] One of our most successful model systems in this context was the Cu(I) complex of a [2]-rotaxane made from 2,9-diphenyl-1,10-phenanthroline (dpp)-incorporating macrocycle threaded onto a dpp-bridged, heterobimetallic Zn(II)/Au(III) bis-porphyrin dumbbell molecular component,[6] schematically represented in Figure 1a. Photoinduced electron transfer from the Zn(II) porphyrin singlet excited state to the Au(III) porphyrin took place at a rate of $(1.7\ \text{ps})^{-1}$ in butyronitrile, very close to the $(3\ \text{ps})^{-1}$ global rate that was observed for the natural system. Furthermore, it was demonstrated that the central metal played a crucial role in effectively controlling the rate of electron transfer between the porphyrin chromophores.[7] In this model molecule, the donor and acceptor porphyrins are linked covalently, and electron transfer may proceed through bond via the dpp bridge or through space via the dpp fragment of the macrocycle, which is interspersed between the two chromophores.

A following step was that of taking advantage of mechanical bonds. To this aim, catenanes[8] and rotaxanes[9,10] were synthesized to study through-space electron transfer. At first, systems involving macrocycles with pendent porphyrins, as schematically represented in Figure 1b and c, were prepared and their photochemical properties investigated.[9]

In this paper, we report on the synthesis, characterization, and photophysical properties of rotaxanes that were made of a macrocycle incorporating a Au(III) porphyrin in its backbone and threaded onto a Zn(II) bis-porphyrin dumbbell component (Figure 1d).[10] In the absence of the central Cu(I) cation, photoinduced electron transfer across mechanical bonds is observed, whereas in the presence of the templating metal, the mechanism and kinetics of electron transfer are very different from those observed in the case of Cu(I) [2]-rotaxane of Figure 1a, despite the fact that both rotaxanes are built from similar photo- and electroactive components.

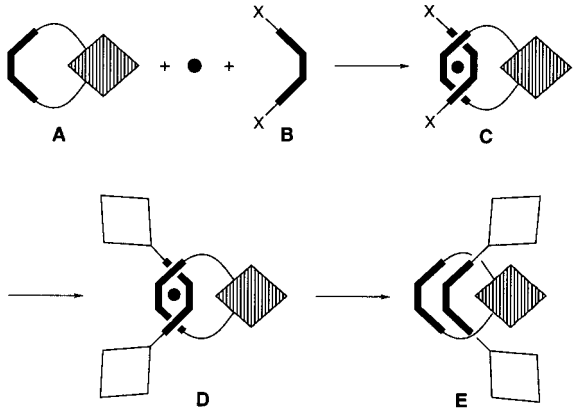

Figure 2. Principle of transition metal-templated synthesis of a [2]-rotaxane containing a Au(III) porphyrin-incorporating macrocycle. Symbols are as in Figure 1. See text for details.

Results and Discussion.

1. Design and Synthesis. 1.1. Principles of Rotaxane Assembly. Rotaxanes made of Au(III) porphyrin-containing macrocycles threaded onto Zn(II) bis-porphyrin dumbbell molecular components were assembled using the transition metal template technique developed for preparing catenanes,[11] rotaxanes,[12] and knots.[13] As shown in Figure 2, the metal controls the threading of the chelating macrocycle (A) onto a complementary chelate (B) ended by functional groups X, to afford a prerotaxane metal complex (C). Subsequent construction of the porphyrin stoppers at the precursor functions X provides the desired [2]-rotaxane structure, as its complex with the metal template (D). Removal of the latter by competitive complexation releases the "free" [2]-rotaxane (E) by suppression of the coordination bonds between the molecular dumbbell and the macrocycle. These components nevertheless remain linked by the so-called *mechanical bond*, which is nothing more than the result of steric interactions between the macrocycle and the stoppers.

1.2. Synthesis of the Precursors and Preparation of the [2]-Rotaxane. The different precursors to the macrocycle and/or the rotaxane of this study are represented in Figure 3. At first, macrocycle $\mathbf{Au}^{+}$, incorporating a Au(III) porphyrin in its backbone, was prepared as follows. 2,9-Bis(*p*-hydroxyphenyl)-1,10-phenanthroline **1**[11b] (1 equiv) was reacted with 2-bromoethanol (3 equivs) in the presence of K_2CO_3 (DMF, 150 °C) to produce crude 2,9-bis[*p*-(2-hydroxyethoxy)phenyl]-1,10-phenanthroline **2**, which was used without purification in the reaction

(5) (a) Harriman, A.; Odobel, F.; Sauvage, J.-P. *J. Am. Chem. Soc.* **1995**, *117*, 9461−9472. (b) Flamigni, L.; Barigelletti, F.; Armaroli, N.; Collin, J.-P.; Sauvage, J.-P.; Williams, J. A. G. *Chem. Eur. J.* **1998**, *4*, 1744−1754. (c) Flamigni, L.; Armaroli, N.; Collin, J.-P.; Dixon, I. M.; Sauvage, J.-P.; Williams, J. A. G. *Coord. Chem. Rev.* **1999**, *190*−*192*, 671−682. (d) Dixon, I. M.; Collin, J.-P.; Sauvage, J.-P.; Barigelletti, F.; Flamigni, L. *Angew. Chem., Int. Ed.* **2000**, *39*, 1292−1295.

(6) Chambron, J.-C.; Harriman, A.; Heitz, V.; Sauvage, J.-P. *J. Am. Chem. Soc.* **1993**, *115*, 6109−6114.

(7) Chambron, J.-C.; Harriman, A.; Heitz, V.; Sauvage, J.-P. *J. Am. Chem. Soc.* **1993**, *115*, 7419−7425.

(8) (a) Amabilino, D. B.; Sauvage, J.-P. *Chem. Commun.* **1996**, 2441−2442. (b) Amabilino, D. B.; Sauvage, J.-P. *New J. Chem.* **1998**, *22*, 395−409.

(9) (a) Linke, M.; Chambron, J.-C.; Heitz, V.; Sauvage, J.-P. *J. Am. Chem. Soc.* **1997**, *119*, 11329−11330. (b) Andersson, M.; Linke, M.; Chambron, J.-C.; Davidsson, J.; Heitz, V.; Sauvage, J.-P.; Hammarström; L. *J. Am. Chem. Soc.* **2000**, *122*, 3526−3527.

(10) Linke, M.; Chambron, J.-C.; Heitz, V.; Sauvage, J.-P.; Semetey, V. *Chem. Commun.* **1998**, 2469−2470.

(11) (a) Dietrich-Buchecker, C.; Sauvage, J.-P. *Chem. Rev.* **1987**, *87*, 795−810. (b) Dietrich-Buchecker, C.; Sauvage, J.-P. *Tetrahedron* **1990**, *46*, 503−512. (c) Sauvage, J.-P. *Acc. Chem. Res.* **1990**, *23*, 327−332.

(12) (a) Chambron, J.-C.; Heitz, V.; Sauvage, J.-P. *J. Chem. Soc., Chem. Commun.* **1992**, 1131−1133. (b) Chambron, J.-C.; Heitz, V.; Sauvage, J.-P. *J. Am. Chem. Soc.*, **1993**, *115*, 12378−12384.

(13) (a) Dietrich-Buchecker, C. O.; Sauvage, J.-P. *Angew. Chem., Int. Ed. Engl.* **1989**, *28*, 189−192. (b) Dietrich-Buchecker, C. O.; Sauvage, J.-P.; Kintzinger, J.-P.; Maltèse, P.; Pascard, C.; Guilhem, J. *New J. Chem.* **1992**, *16*, 931−942. (c) Dietrich-Buchecker, C. O.; Nierengarten, J.-F.; Sauvage, J.-P.; Armaroli, N.; Balzani, V.; De Cola, L. *J. Am. Chem. Soc.* **1993**, *115*, 11237−11244. (d) Carina, R.; Dietrich-Buchecker, C.; Sauvage, J.-P. *J. Am. Chem. Soc.* **1996**, *118*, 9110−9116. (e) Dietrich-Buchecker, C. O.; Sauvage, J.-P.; De Cian, A.; Fischer, J. *J. Chem. Soc., Chem. Commun.* **1994**, 2231−2232.

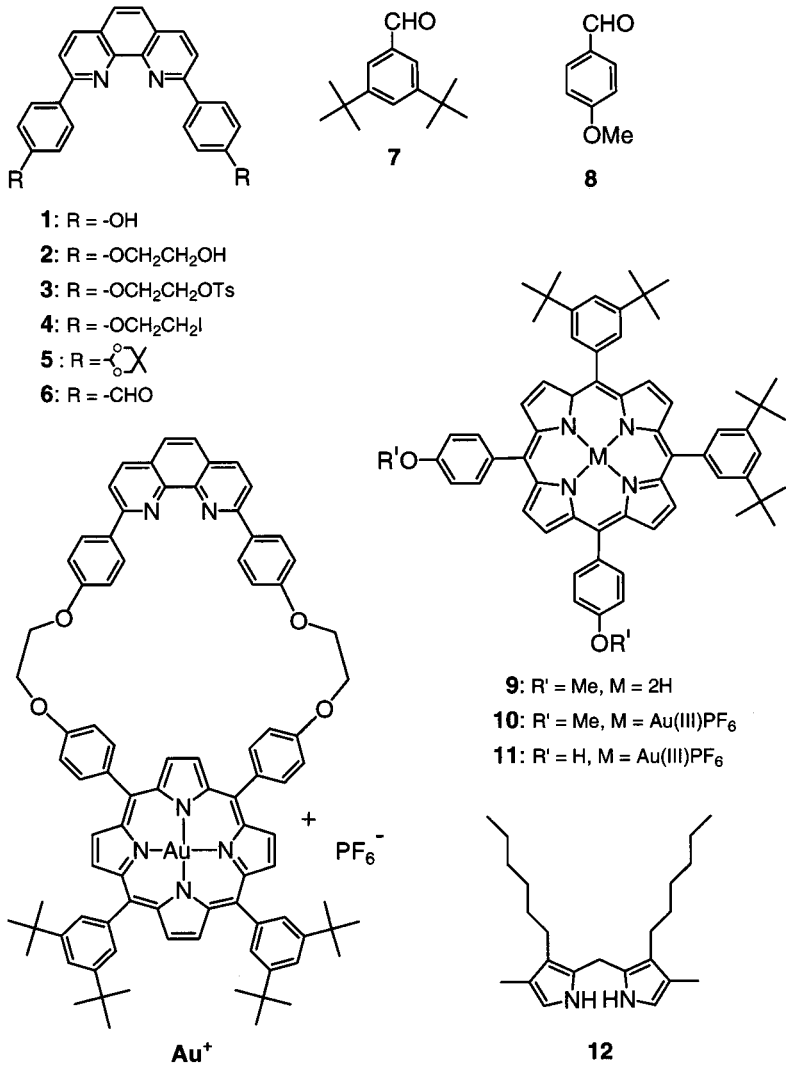

Figure 3. Chemical formulas of the precursors of the [2]-rotaxane.

with tosyl chloride (Et_3N, CH_2Cl_2, 0 °C). The overall yield of ditosylate **3** was 31% after chromatography. Exchange of the tosylate functional groups of **3** by iodide (NaI, refluxing acetone) yielded quantitatively the phenanthroline derivative **4**. The porphyrin precursor was prepared following Lindsey's procedure[14] using 3,5-di-*tert*-butylbenzaldehyde **7**[15] (1 equiv), 4-methoxybenzaldehyde **8** (1 equiv), and pyrrole (2 equivs). 15,20-bis(3,5-di-*tert*-butylphenyl)-5,10-bis(4-methoxyphenyl)-porphyrin **9** was isolated in 6% yield after chromatographic separation from the other porphyrins produced in this reaction. Au(III) was then inserted by reaction of **9** with $KAuCl_4$ (2 equivs) in the presence of NaOAc (2.5 equivs) in refluxing acetic acid.[4b] The Au(III) complex **10** of free base porphyrin **9** was isolated in nearly quantitative yield as its PF_6^- salt. The methoxy groups were cleaved by BBr_3 (30 equivs) in CH_2Cl_2 at −78 °C, affording the Au(III) porphyrin **11** quantitatively. Finally, the coupling reaction of phenanthroline derivative **4** (1.1 equivs) and Au(III) porphyrin **11** (1 equiv) in the presence of Cs_2CO_3 (DMF, 55 °C) afforded macrocycle $\mathbf{Au}^+$ as its PF_6^- salt in 31% yield.

2,9-Bis[*p*-(formylphenyl)]-1,10-phenanthroline **6**[15] of this study was prepared from commercial 1,10-phenanthroline in two steps. First, reaction of 2.5 equivs of *p*-(5,5-dimethyl-1,3-dioxan-2-yl)lithiobenzene[16] with 1,10-phenanthroline, followed by hydrolysis and rearomatization with excess MnO_2 afforded 2,9-bis[*p*-(5,5-dimethyl-1,3-dioxan-2-yl)phenyl]-1,10-phenanthroline **5** in 47% yield after column chromatography. The desired dialdehyde **6** was recovered in 95% yield by acidic hydrolysis of **5**.

Template formation of prerotaxane $\mathbf{Cu}^+\mathbf{Au}^+$ of Figure 4 was carried out by mixing macrocycle $\mathbf{Au}^+$ with equimolecular amounts of $Cu(CH_3CN)_4PF_6$ and 2,9-bis[*p*-(formylphenyl)]-1,10-phenanthroline **6**. Prerotaxane $\mathbf{Cu}^+\mathbf{Au}^+$ was obtained quantitatively and used directly in the next step. Porphyrin stoppers were constructed at the protruding aldehyde functions as follows (Figure 4): a mixture of prerotaxane $\mathbf{Cu}^+\mathbf{Au}^+$ (1 equiv), 3,5-di-*tert*-butylbenzaldehyde **7**[15] (8 equivs), (3,3′-dihexyl-4,4′-dimethyl-2,2′-dipyrryl)methane **12** (10 equivs),[17] and a few drops of trifluoroacetic acid in CH_2Cl_2 was stirred at RT overnight. Tetrapyrrole assembly was fixed by controlled oxidation of the porphyrinogens with tetrachloro-*p*-benzoquinone in refluxing CH_2Cl_2. Cu(I)-complexed [2]-rotaxane $\mathbf{(H_2)_2Cu}^+\mathbf{Au}^+$ was isolated in 13% yield after chromatographic purification. Free base porphyrin $\mathbf{H_2}$ was also isolated from the

(14) (a) Lindsey, J. S.; Hsu, H. C.; Schreiman, I. C. *Tetrahedron Lett.* **1986**, *27*, 4969−4970. (b) Lindsey, J. S.; Schreiman, I. C.; Hsu, H. C.; Kearney, P. C.; Marguerettaz, A. M. *J. Org. Chem.* **1987**, *52*, 827−836. (c) Lindsey, J. S.; Wagner, R. W. *J. Org. Chem.* **1989**, *54*, 828−836.

(15) Chardon-Noblat, S.; Sauvage, J.-P. *Tetrahedron* **1991**, *47*, 5123−5132.

(16) Solladié, N.; Chambron, J.-C.; Sauvage, J.-P. *J. Am. Chem. Soc.* **1999**, *121*, 3684−3692.

(17) (a) Arsenault, G. P.; Bullock, E.; McDonald, S. F. *J. Am. Chem. Soc.* **1960**, *82*, 4384−4389. (b) Young, R.; Chang, C. K. *J. Am. Chem. Soc.* **1985**, *107*, 898−909.

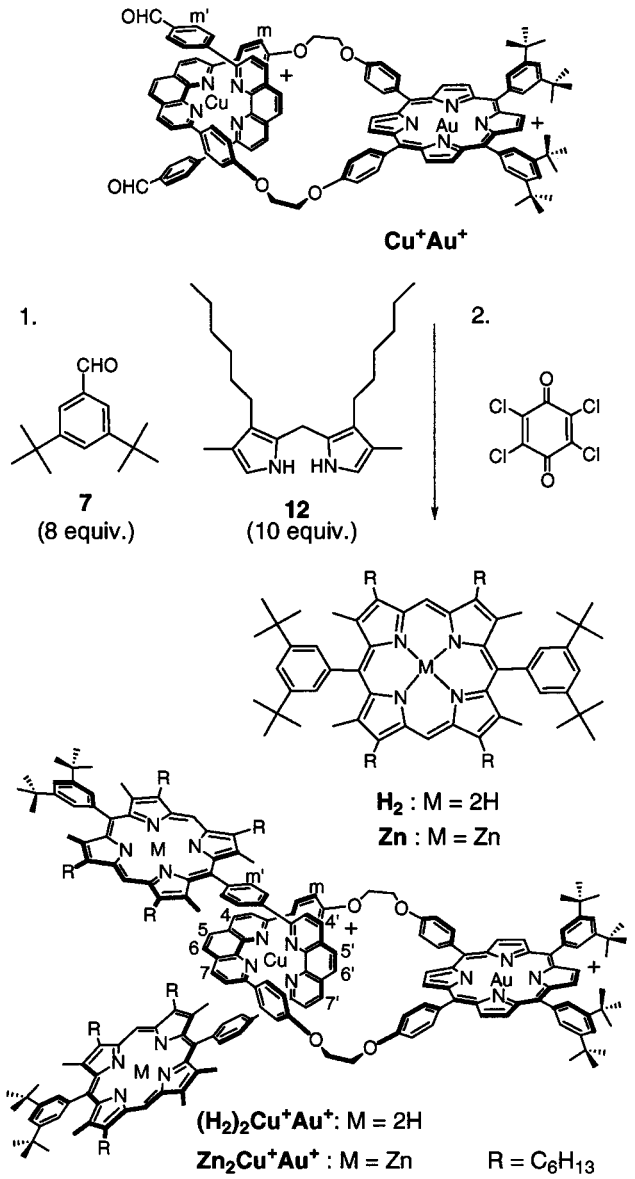

Figure 4. Cu(I)-directed template synthesis of [2]-rotaxane $\mathbf{Zn_2Cu^+Au^+}$.

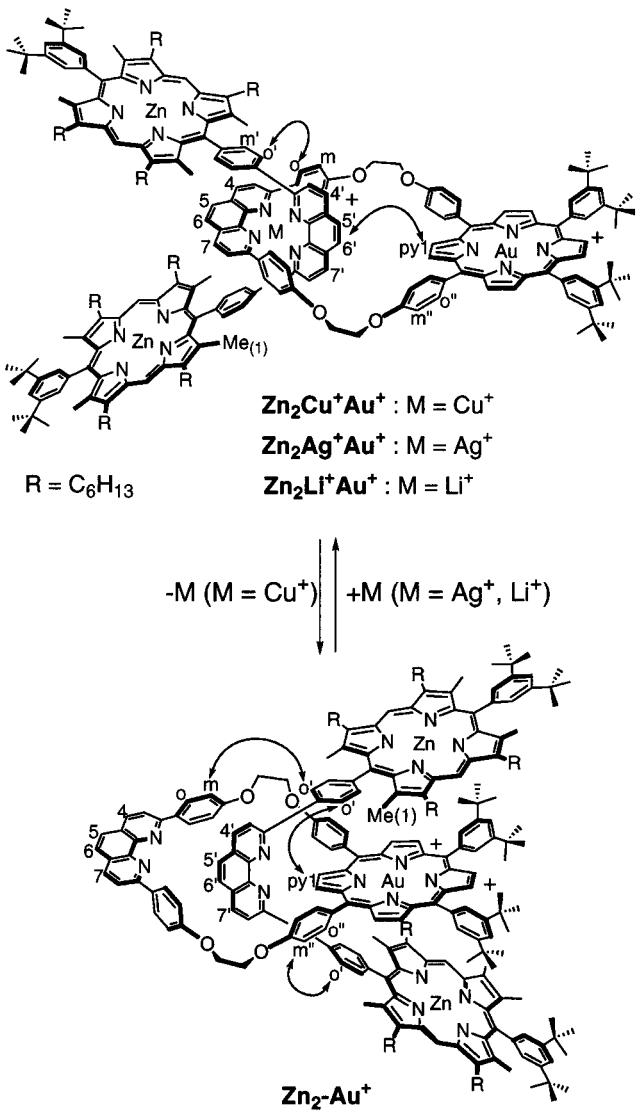

Figure 5. Illustration of the demetalation/remetalation reactions carried out on Cu(I)-complexed [2]-rotaxane $\mathbf{Zn_2Cu^+Au^+}$ to afford free [2]-rotaxane $\mathbf{Zn_2{-}Au^+}$ and metallo-[2]-rotaxanes $\mathbf{Zn_2Ag^+Au^+}$ and $\mathbf{Zn_2Li^+Au^+}$ and showing the pirouetting motion of the Au(III)-incorporating macrocycle upon removal of the central metal. Indicated with arrows are the rOe correlations as observed by proton NMR spectroscopy.

reaction mixture. Zn(II) insertion into the porphyrin stoppers of $\mathbf{(H_2)_2Cu^+Au^+}$ was performed by reaction with $Zn(OAc)_2 \cdot 2H_2O$ in a refluxing mixture of $CHCl_3$ and CH_3OH and afforded nearly quantitatively Cu(I)-complexed [2]-rotaxane $\mathbf{Zn_2Cu^+Au^+}$. Reference porphyrin **Zn** was obtained similarly.

1.3. Formation of the Free [2]-Rotaxane and Coordination Chemistry Studies. The metal template (Cu(I)) was selectively extruded by reacting the [2]-rotaxane complex $\mathbf{Zn_2Cu^+Au^+}$ with KCN (50 equivs) in a 1:1:4 mixture of $CHCl_3$, H_2O, and CH_3CN at 40 °C for 30 min.[18] This decomplexation reaction liberated the free [2]-rotaxane $\mathbf{Zn_2{-}Au^+}$ quantitatively. As studied in more detail in the next section, and depicted in Figure 5, the template imprint (a bis-dpp, tetrahedral coordination sphere) is completely vanished by rearrangement of the threaded macrocycle around its axle. Recomplexation of $\mathbf{Zn_2{-}Au^+}$ with Ag^+ or Li^+ by reaction with $AgBF_4$ or $LiBF_4$ restored the template imprint and afforded the Ag^+- and Li^+-[2]-rotaxane complexes $\mathbf{Zn_2Ag^+Au^+}$ and $\mathbf{Zn_2Li^+Au^+}$ quantitatively.

2. Conformations of the [2]-Rotaxanes in Solution: a Proton NMR Study. 2.1. Dichloromethane Solution. In this section, we compare the conformations of [2]-rotaxane $\mathbf{Zn_2{-}Au^+}$ and its metal complexes, $\mathbf{Zn_2Cu^+Au^+}$, $\mathbf{Zn_2Ag^+Au^+}$, and $\mathbf{Zn_2Li^+Au^+}$. We show that removal of the metal template is followed by a pirouetting motion of the macrocyclic component, placing the Au(III) porphyrin that it incorporates in the cleft formed by the two Zn(II) porphyrin stoppers. For the sake of comparison, the data obtained earlier for the prototypical Cu(I) [2]-catenate $\mathbf{Cu^{+}}$[11b] and the related Cu(I) [2]-rotaxane $\mathbf{(H_2)_2Cu^+}$,[19a] as well as its dumbbell precursor $\mathbf{(H_2)_2}$[19b] (Figure 6) will be included in this study. Relevant data are collected in Table 1. The chart shows the proton labeling of the different components of the rotaxanes. Protons relevant to the following discussion are highlighted in Figures 4−6. Let us follow the sequence of reactions shown in Figures 4 and 5. Diagnosis of

(18) (a) Albrecht-Gary, A.-M.; Saad, Z.; Dietrich-Buchecker, C. O.; Sauvage, J.-P. *J. Am. Chem. Soc.* **1985**, *107*, 3205−3209. (b) Dietrich-Buchecker, C. O.; Sauvage, J.-P.; Kern, J.-M. *J. Am. Chem. Soc.* **1984**, *106*, 3043−3045.

(19) (a) Chambron, J.-C.; Heitz, V.; Sauvage, J.-P. *Bull. Soc. Chim. Fr.* **1995**, *132*, 340−347. (b) Hungerford, G.; Van der Auweraer, M.; Chambron, J.-C.; Heitz, V.; Sauvage, J.-P.; Pierre, J.-L.; Zurita, D. *Chem. Eur. J.* **1999**, *5*, 2089−2100.

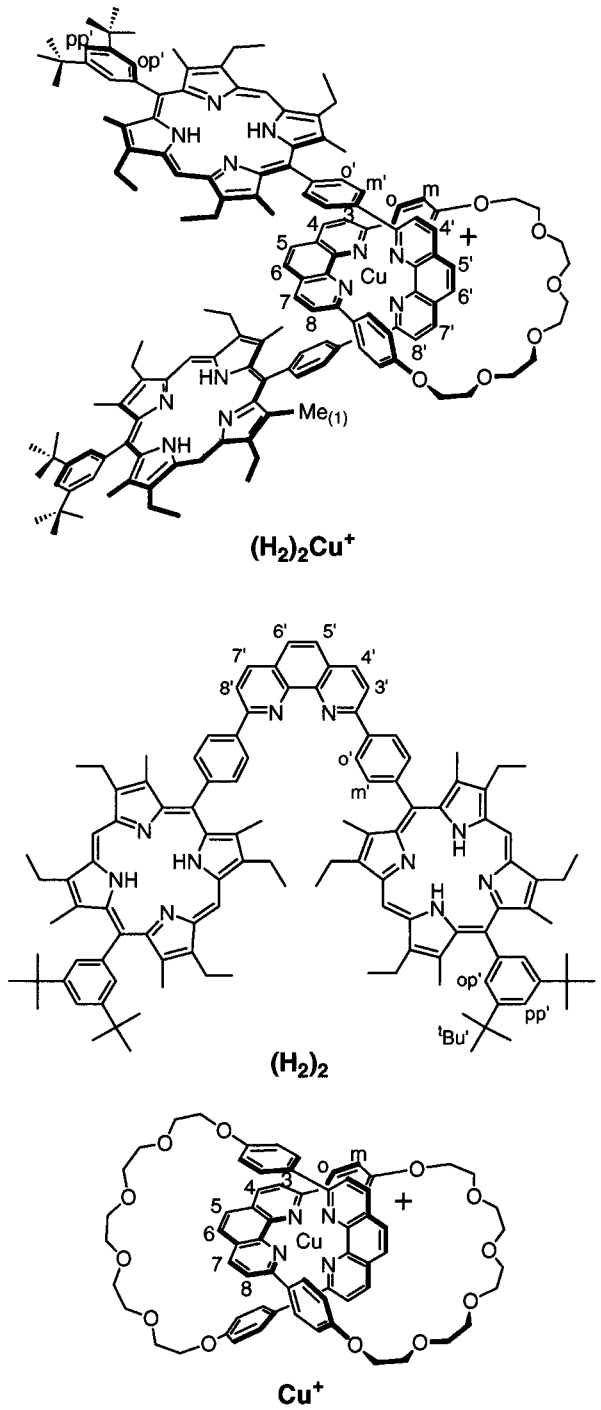

Figure 6. Chemical structures of the reference bisporphyrin $(\mathbf{H_2})_2$, [2]-rotaxane $(\mathbf{H_2})_2\mathbf{Cu}^+$, and Cu(I) [2]-catenate $\mathbf{Cu}^+$.

successful Cu(I)-directed threading of macrocycle $\mathbf{Au}^+$ onto dialdehyde **6** to afford prerotaxane $\mathbf{Cu}^+\mathbf{Au}^+$ is the observation of a high-field signal at 6.36 ppm for the protons m of $\mathbf{Au}^+$,[20] as in [2]-catenate $\mathbf{Cu}^+$ (6.02 ppm).[11b] The same threading process accounts for the −1.0 and −0.5 ppm upfield shifts of the m′ and CHO protons, respectively, which are embedded in the shielding field of the phenanthroline fragment of $\mathbf{Au}^+$. However, the doublet of the m′ protons (7.10 ppm) appears at lower field than the m protons in $\mathbf{Cu}^+\mathbf{Au}^+$ (6.36 ppm) because of the deshielding effect of the CHO group. A stronger effect exerted by the porphyrins on their meso substituents accounts for the further shift of the m′ protons to 7.50 ppm in Cu(I) [2]-rotaxane species $(\mathbf{H_2})_2\mathbf{Cu}^+\mathbf{Au}^+$. Comparison of free base [2]-rotaxanes $(\mathbf{H_2})_2\mathbf{Cu}^+$ and $(\mathbf{H_2})_2\mathbf{Cu}^+\mathbf{Au}^+$ (Figures 4 and 6) shows that all of the chemical shifts of the dumbbell protons are similar, except for those of the pairs (5′,6′) and (4′,7′), which are shielded by −0.62 and −0.19 ppm respectively, on going from an "innocent" to the Au(III) porphyrin-incorporating macrocycle. Therefore, it is not surprising that the most affected protons are those located in the vicinity of the Au(III) porphyrin, that is, those belonging to the "rear" part of the dumbbell component. We suggest that this shielding is due to the fact that the proton pairs (5′,6′) and (4′,7′) are placed above the Au(III) porphyrin plane, a situation that could be made possible by a folding of the macrocycle (not represented in the figures). Incorporation of Zn(II) into the porphyrin stoppers does not significantly alter the chemical shifts (compare $(\mathbf{H_2})_2\mathbf{Cu}^+\mathbf{Au}^+$ and $\mathbf{Zn_2Cu}^+\mathbf{Au}^+$), as expected. The same is true for the exchange of Ag^+ or Li^+ for Cu^+: all of the metallorotaxanes, $\mathbf{Zn_2Cu}^+\mathbf{Au}^+$, $\mathbf{Zn_2Ag}^+\mathbf{Au}^+$, and $\mathbf{Zn_2Li}^+\mathbf{Au}^+$, have very similar spectra. Comparison of the data of catenate $\mathbf{Cu}^+$ and rotaxanes $(\mathbf{H_2})_2\mathbf{Cu}^+$ and $(\mathbf{H_2})_2\mathbf{Cu}^+\mathbf{Au}^+$ (Figures 4 and 6) shows that the signals of the proton pairs (5,6) and (4,7) belonging to the dpp portion of the macrocycles are moved upfield upon passing from $\mathbf{Cu}^+$ to the rotaxanes. This result clearly demonstrates that, in the case of $(\mathbf{H_2})_2\mathbf{Cu}^+\mathbf{Au}^+$, the phenanthroline nucleus incorporated in the macrocycle is, at least partially, embedded in the shielding field of the porphyrin stoppers, which is in agreement with the proposed structure (Figure 4).

Drastic modifications of the proton NMR spectrum are observed upon demetalation of the central coordination site, due to a complete changeover of the molecule (Figure 5). Protons o′, m′, and $Me_{(1)}$ of the dumbbell fragment experience a downfield shift of +1.02, +0.64, and +0.43 ppm, respectively, whereas the pair (4′,7′) is moved upfield by −0.44 ppm. Upfield shifts are also observed for pairs (4,7) (−0.20 ppm), and (5,6) (−0.29 ppm) and protons o″ (−0.21 ppm), and py_1 (−0.50 ppm) of the macrocycle, whereas o and m of the same component are moved downfield by ∼+0.70 ppm. These data support the following picture of free [2]-rotaxane $\mathbf{Zn_2}-\mathbf{Au}^+$: the macrocycle has executed a pirouetting motion, placing the Au(III) porphyrin in the cleft formed by the two Zn(II) porphyrins of the dumbbell. Hence, the result is the upfield shifts of o″ and py_1, which are likely to be the most efficiently embedded in the shielding field of the Zn(II) porphyrin stoppers. Upfield shifts of the proton pairs (4,7) and (5,6) are due to electronic effects: coordination of Cu(I) to dpp is known to produce downfield shifts of +0.22 and +0.26 ppm, respectively.[21] On the other hand, downfield shifts of the pairs (o,m) and (o′,m′), ranging from +0.64 to +1.02 ppm, are due to the fact that upon demetalation, the phenylene spacers become coplanar with the phenanthroline nuclei.[21]

All of these interpretations, which rely on shielding and deshielding effects, are also supported by 2D ROESY experiments. Remarkable rOe cross-peaks can be found in the NMR maps that correspond to dipolar couplings between protons of the macrocycle on one hand and protons of the dumbbell component on the other hand. In the case of the Cu(I) complex $\mathbf{Zn_2Cu}^+\mathbf{Au}^+$, correlations (see Figure 5) are observed between protons o and o′, as well as between (5′,6′) and py_1. In the case of the free [2]-rotaxane $\mathbf{Zn_2}-\mathbf{Au}^+$, the correlations observed for the complex give place to correlations between protons o′

(20) Comparison to free macrocycle $\mathbf{Au}^+$ is not useful because the spectrum of the latter is concentration-dependent, as observed previously for a related macrocycle (see ref 8b).

(21) Dietrich-Buchecker, C. O.; Marnot, P. A.; Sauvage, J.-P.; Kintzinger, J.-P.; Maltèse, P. *Nouv. J. Chim.* **1984**, *8*, 573−582.

Table 1: Selected ^{1}H NMR Data for the Rotaxanes and Reference Compounds[a]

	dumbell protons							macrocycle protons								
compd	5′,6′	4′,7′	3′,8′	o′	m′	$Me_{(1)}$	meso	5,6	4,7	3,8	o	m	m″	o″	$py_{(1)}$	$py_{(2)}$
Cu^{+}[11b]								8.28	8.66	7.87	7.37	6.02				
6	7.88	8.40	8.23	8.63	8.12		10.16[b]									
$(H_2)_2$[19b]	7.96	8.52	8.52	9.02	8.30	2.41	10.17									
$(H_2)_2Cu^{+}$[19a]	8.57	9.07	8.41	8.03	7.44	1.81	10.19	7.54	8.39	8.11	7.55	6.24				
$Cu^{+}Au^{+}$	7.80	8.67	8.08	7.60	7.10		9.66[b]	7.90	8.45	7.87	7.34	6.36	7.68	8.34	9.27	9.54
$(H_2)_2Cu^{+}Au^{+}$	7.95	8.88	8.50	8.11	7.50	1.72	10.14	7.72	8.26	7.92	7.58	6.60	7.74	8.39	9.26	9.57
$Zn_2Cu^{+}Au^{+}$	7.98	8.90	8.52	8.13	7.54	1.84	10.13	7.75	8.31	7.97	7.62	6.63	7.78	8.42	9.30	9.60
$Zn_2Ag^{+}Au^{+}$	7.99	8.82	8.56	8.19	7.58	1.79	10.10	7.49	8.18	7.93	7.79	6.65	7.75	8.42	9.26	9.61
$Zn_2Li^{+}Au^{+}$	7.94	8.90	8.48	8.07	7.53	1.74	10.12	7.71	8.23	7.84	7.53	6.67	7.82	8.42	9.29	9.60
Zn_2-Au^{+}	7.90	8.46	8.57	9.15	8.18	2.27	10.07	7.46	8.11	7.99	8.26	7.39	7.91	8.21	8.80	9.56

[a] Chemical shifts in ppm downfield from TMS. Solvent: CD_2Cl_2. [b] C*H*O proton.

Chart 1

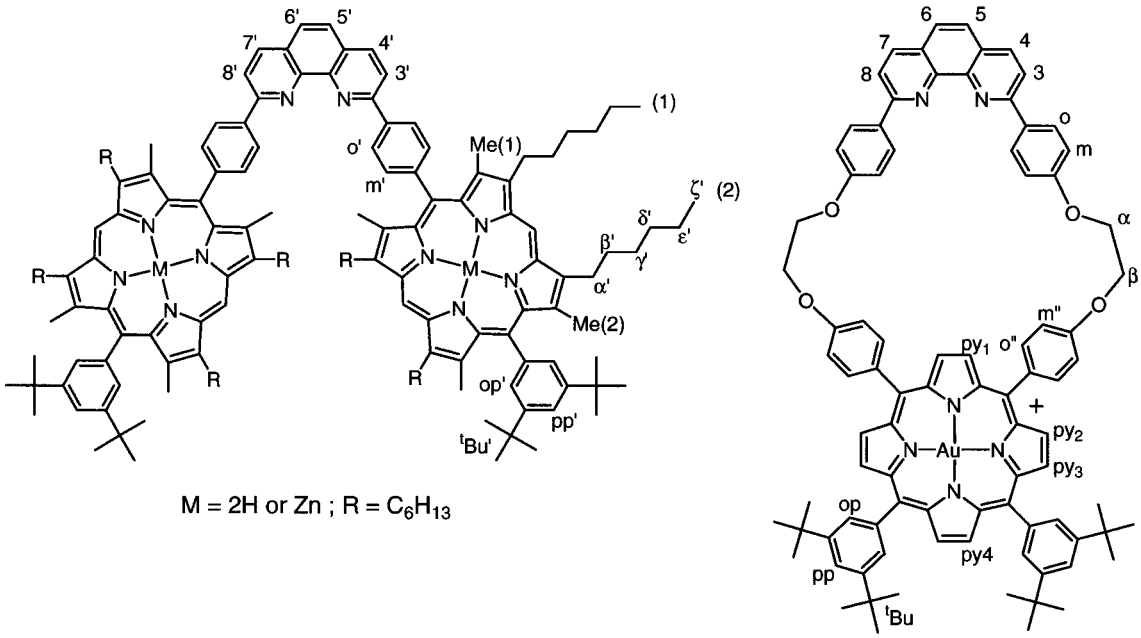

and m, o′ and py_1, and o′ and m″ which are fully consistent with the structures depicted in Figure 5.

2.2. Acetonitrile Solution. In addition to photochemical investigations that were performed in nitrile solutions, ^{1}H NMR studies were also carried out on the free [2]-rotaxane **Zn_2-Au^{+}** in acetonitrile. At 40 °C, all the peaks were broad. It was necessary to heat the sample solution to 74 °C to observe significant peak sharpening and resolution of most of the proton signals. However, over the 40−74 °C temperature range, there was no dramatic change in the general appearance of the whole spectrum. Signals of the probe protons of the CD_2Cl_2 study were not dramatically shifted in CD_3CN. Indeed, with the exception of protons m, which undergo a −0.49 ppm upfield shift, the probe protons were very little affected by the solvent change; that is, o′, −0.18 ppm; py_1, +0.13 ppm; and $Me_{(1)}$, +0.08 ppm. This suggests that, at least in CD_3CN at 74 °C, the conformation of **Zn_2-Au^{+}** is very similar to the one observed in CD_2Cl_2 at room temperature. Peak broadening at lower temperatures could be indicative of relatively slow exchange between conformations. If the driving force for bringing the gold porphyrin cation between the two zinc porphyrins is due to ion−dipole interactions, these are expected to drop in the more polar acetonitrile solvent, allowing for the existence of an extended conformation in free [2]-rotaxane **Zn_2-Au^{+}**. Indeed, as shown in section 4, combined time-resolved and steady-state spectroscopy techniques will allow drawing quite a detailed picture of the conformational behavior of **Zn_2-Au^{+}** in acetonitrile.

3. Electrochemistry Studies of the [2]-Rotaxanes and their Models. Table 2 shows selected redox potentials measured in butyronitrile for the rotaxanes **$Zn_2Cu^{+}Au^{+}$** and **Zn_2-Au^{+}**, as well as for the model compounds **Cu^{+}**, **Zn**, **Au^{+}** and prerotaxane **$Cu^{+}Au^{+}$**. Only the redox potentials obtained for the first oxidation processes of the zinc porphyrin and copper complex subunits and the first reduction process of the gold porphyrin macrocycle are of interest here to establish the ergonicity of the various electron-transfer processes and the energy content of the charge-separated products. Also shown are the excited-state redox potentials that were calculated using the present data and the corresponding values of the excited-state energies (see Table 4) and neglecting Coulombic effects.

Remarkably, the values measured for the porphyrinic model compounds are found unchanged in the rotaxanes, which shows that the positive charge of the central Cu(I) complex has no influence on the neighboring porphyrins, which behave independently.

In the case of the different compounds incorporating a gold porphyrin subunit, the first reduction wave, which is reversible, is observed at ∼−1.04 V vs $Fc^{+/0}$. It corresponds to the reduction of the Au(III) porphyrin cation to the corresponding neutral radical: the Au(III) porphyrin is the easiest reducible

Table 2: Electrochemical Data for the Rotaxanes and the Reference Compounds

	ground-state redox potentials[a]			excited-state redox potentials[b]			
compd	Cu^{2+}/Cu^{+}	$Zn^{+\bullet}/Zn$	$Au^{+}/Au^{\bullet}$	Cu^{2+}/Cu^{+*}	$Zn^{+\bullet}/{}^{1}Zn^{*}$	$Zn^{+\bullet}/{}^{3}Zn^{*}$	$^{3}Au^{+*}/Au^{\bullet}$
Cu^{+}	0.14 (70)						
Zn		0.17 (65)			−1.95	−1.54	
Au^{+}			−1.03 (50)				0.70
Cu^{+}**Au**$^{+}$	0.37 (100)		−1.02 (60)	−1.40			0.71
Zn$_2$Cu^{+}**Au**$^{+}$	0.43 (140)	0.18 (60)	−1.04 (65)	−1.34	−1.94	−1.52	0.71
Zn$_2$−**Au**$^{+}$		0.17 (70)	−1.05 (65)		−1.95	−1.53	0.70

[a] V vs $Fc^{+/0}$ (ΔE_p, mV). 0.1 M TBAB in butyronitrile. [b] Calculated by subtracting the excited-state energy level from the corresponding ground-state redox potential.

Table 3. Absorption Maxima in the Visible Region[a]

	λ_{max} (nm) ($\epsilon \times 10^{-5}$ [M^{-1} cm^{-1}])		
Zn[b]	415 (3.10)	543 (0.17)	576 (0.07)
Au^{+}	415 (1.86)	525 (0.14)	560 (0.04)
Cu^{+}	425 (0.02)		
Zn$_2$−**Au**$^{+}$	415 (5.51)	540 (0.35)	574 (0.12)
Zn$_2$Cu^{+}**Au**$^{+}$	415 (7.83)	541 (0.41)	573 (0.13)

[a] In acetonitrile, except otherwise specified. [b] In butyronitrile/acetonitrile (1/1).

redox subunit and, therefore, is the best electron acceptor. As expected, oxidation of the Zn porphyrin subunits takes place at 0.17 V vs $Fc^{+/0}$. Oxidation of the central Cu(I) complex is found at +0.37 vs $Fc^{+/0}$ for prerotaxane **Cu**$^{+}$**Au**$^{+}$ and +0.43 V vs $Fc^{+/0}$ for [2]-rotaxane **Zn$_2$Cu**$^{+}$**Au**$^{+}$. These values are 230−290 mV more positive than that of the model compound **Cu**$^{+}$. Examination of the literature data shows that the oxidation potentials of copper(I) bis-phenanthroline complexes range from 0.045 to 1.175 V vs $Fc^{+/0}$ (0.42 to 1.55 V vs SCE[22]), depending on both the electronic and steric effects of the substituents anchored to the 1,10-phenanthroline ligand.[23−25] In particular, bulky substituents enforcing a tetrahedral geometry, particularly 2,9-substituents[24,25], or electron-withdrawing groups, such as CF_3[26] raise the Cu(II)/Cu(I) potential by the stabilization of the Cu(I) redox state. The present data can be explained in this frame.

Inspection of the excited-state redox potentials shows that the Zn porphyrin excited state (singlet or triplet) can transfer an electron to the Au(III) porphyrin ground state ($\Delta G = -0.90$ eV and −0.48 eV, respectively), whereas the triplet Au(III) porphyrin excited state can abstract an electron from the Zn porphyrin ($\Delta G = -0.53$ eV). The energy levels of the corresponding charge-separated states, namely $^{+\bullet}$**Zn$_2$Cu**$^{+}$**Au**$^{\bullet}$ and $^{+\bullet}$**Zn$_2$**−**Au**$^{\bullet}$ can be estimated to lie at 1.22 eV. Importantly, the Au(III) porphyrin in its ground state can also be reduced by the central Cu(I) complex in its excited state (MLCT in nature). The resulting charge-separated state, **Zn$_2$Cu**$^{2+}$**Au**$^{\bullet}$, lies at the energy level of 1.47 eV. As a consequence of the relatively high Cu(II/I) redox potential, $E(Cu^{2+}/Cu^{+}) > E(Zn^{+\bullet}/Zn)$; therefore, the state **Zn$_2$Cu**$^{2+}$**Au**$^{\bullet}$ can be converted into the fully charge-separated state $^{+\bullet}$**Zn$_2$Cu**$^{+}$**Au**$^{\bullet}$ by a charge shift from the Zn porphyrin to the oxidized central Cu(II) complex.

4. Photophysical Properties of the Rotaxanes Zn$_2$−Au^{+} and Zn$_2$Cu^{+}Au^{+}. The spectroscopic and photophysical properties of the models **Zn**, **Au**$^{+}$, and **Cu**$^{+}$ are collected in Tables 3 (absorption), 4 (emission), and 5 (transient absorption), together with those of the rotaxanes **Zn$_2$**−**Au**$^{+}$ and **Zn$_2$Cu**$^{+}$**Au**$^{+}$, and are in agreement with those of related compounds.[27−30] As shown in Figure 7, the absorption spectrum of **Zn$_2$Cu**$^{+}$**Au**$^{+}$ closely matches the addition of the separate components. The same is true for [2]-rotaxane **Zn$_2$**−**Au**$^{+}$. Therefore, there are few, if any, interactions between the different chromophores in the ground state of the rotaxanes.

4.1 Luminescence Properties. The emission of the zinc porphyrin-based singlet excited state is strongly quenched in rotaxanes **Zn$_2$Cu**$^{+}$**Au**$^{+}$ and **Zn$_2$**−**Au**$^{+}$ at 293 or 77 K. The RT quenching process occurs to a rather different extent (Figure 8) for both compounds. Time-resolved experiments ($\lambda_{exc} = 532$ nm) indicate similar lifetimes for the quenched luminescence: 180 ps for **Zn$_2$Cu**$^{+}$**Au**$^{+}$ and 170 ps for **Zn$_2$**−**Au**$^{+}$, respectively. In addition, although in the case of **Zn$_2$Cu**$^{+}$**Au**$^{+}$ the calculated radiative rate constant ($k_r = \Phi_F/\tau = 4.5 \times 10^6$ s^{-1}) is in reasonable agreement with that of the model **Zn** ($k_r = 5.4 \times 10^6$ s^{-1}), in the case of **Zn$_2$**−**Au**$^{+}$, it is about 30% that of the model (1.7×10^6 s^{-1}).

This apparent discrepancy can be explained on the basis of at least two conformations for **Zn$_2$**−**Au**$^{+}$ (Scheme 1): an extended one, bringing the gold and zinc porphyrin nuclei to a large distance from one another [**Zn$_2$**−**Au**$^{+}$**(l)**, l standing for "long"] and a compact conformation, for which these components are likely to be in close proximity [**Zn$_2$**−**Au**$^{+}$**(s)**, s standing for "short"].[31] The luminescence results can be interpreted if an "immediate" (that is, static) quenching of the zinc porphyrin emission occurs for **Zn$_2$**−**Au**$^{+}$**(s)** faster than our time resolution. By contrast, in the case of **Zn$_2$Cu**$^{+}$**Au**$^{+}$, no static quenching can be evidenced. From the time-resolved data and by comparing the emission quantum yields of **Zn$_2$Cu**$^{+}$-**Au**$^{+}$ and **Zn$_2$**−**Au**$^{+}$ (Table 4), it turns out that the fraction of "immediately" quenched molecules of **Zn$_2$**−**Au**$^{+}$, those in the **Zn$_2$**−**Au**$^{+}$**(s)** conformation, is ca. 70%. The remaining 30% correspond to **Zn$_2$**−**Au**$^{+}$**(l)**, whose emission properties are identical to those of the extended complex, **Zn$_2$Cu**$^{+}$**Au**$^{+}$.

4.2 Transient Absorption Spectroscopy. Transient absorption spectra were obtained at the end of a 35-ps laser pulse (532

(22) Note that, with few exceptions, most of the redox potentials of copper(I) bisphenanthroline complexes have been reported vs SCE in CH_3CN, which makes direct comparisons to the present systems difficult. However, data vs SCE can be converted vs $Fc^{+/0}$, taking into account the fact that the redox potential of the $Fc^{+/0}$ couple in CH_3CN is +0.375 V vs SCE (J.-M. Kern, personal communication).

(23) Miller, M. T.; Gantzel, P. K.; Karpishin, T. B. *Inorg. Chem.* **1999**, *38*, 3414−3422.

(24) Federlin, P.; Kern, J.-M.; Rastegar, A.; Dietrich-Buchecker, C.; Marnot, P.; Sauvage, J.-P. *New J. Chem.* **1990**, *14*, 9−12.

(25) Eggleston, M. K.; McMillin, D. R.; Koenig, K. S.; Pallenberg, A. J. *Inorg. Chem.* **1997**, *36*, 172−176.

(26) Miller, M. T.; Gantzel, P. K.; Karpishin, T. B. *Angew. Chem., Int. Ed.* **1998**, *37*, 1556−1558.

(27) Flamigni, L.; Armaroli, N.; Barigelletti, F.; Chambron, J.-C.; Solladié N.; Sauvage J.-P. *New J. Chem.* **1999**, *23*, 1151−1158.

(28) Flamigni, L.; Barigelletti, F.; Armaroli, N.; Ventura, B.; Collin, J.-P.; Sauvage, J.-P.; Williams, J. A. G. *Inorg. Chem.* **1999**, *38*, 661−667.

(29) Armaroli, N.; De Cola, L.; Balzani, V.; Sauvage, J.-P.; Dietrich-Bucheker, C. O.; Kern, J.-M.; Bailal, A. *J. Chem. Soc., Dalton Trans.* **1993**, 3241−3247.

(30) Armaroli, N.; Rodgers, M. A. J.; Ceroni, P.; Balzani, V.; Dietrich-Bucheker, C. O.; Kern, J.-M.; Bailal, A.; Sauvage, J.-P. *Chem. Phys. Lett.* **1995**, *241*, 555−558.

(31) The structure of the conformation **Zn$_2$**−**Au**$^{+}$**(l)** is tentatively suggested to be similar to that of the array **Zn$_2$Cu**$^{+}$**Au**$^{+}$, but with a lower distance between the zinc- and gold-porphyrin groups, which is allowed by a looser structure than that in **Zn$_2$Cu**$^{+}$**Au**$^{+}$.

Table 4. Emission Properties at 298 K[a] and 77 K[b,c]

		298 K			77 K		
		λ_{max} (nm)	τ (ns)	Φ_F	λ_{max} (nm)	τ (ns)	E(eV)
Zn[c]	^{1}Zn	586	1.84	0.01	584	2.5	2.12
	^{3}Zn				726	54×10^6	1.71
$\mathbf{Au}^+$	^{3}Au$^+$				718	15 000; 10^5	1.73
$\mathbf{Cu}^+$	*Cu$^+$	710	85	0.0003	700		1.77
$\mathbf{Zn_2}$–$\mathbf{Au}^+$	^{1}Zn	586	0.170(90%)−0.580(10%)[e]	0.0003	584	0.300(70%)−2.2(30%)[f]	2.12
	^{3}Au[g]				710	11 000; 10^5	1.75
	^{3}Zn				728	20×10^6	1.70
$\mathbf{Zn_2Cu}^+\mathbf{Au}^+$	^{1}Zn	586	0.180	0.0008	584	0.630(75%)−2.6(25%)[f]	2.12
	^{3}Au				710	15 000; 9×10^4	1.75
	^{3}Zn				728	52×10^6	1.70

[a] In acetonitrile, except otherwise specified. [b] Butyronitrile. [c] In the second column, the excited state is specified. [d] Acetonitrile/butyronitrile (1/1). [e] The 580-ps component, which accounts for 3% of the total ^{1}Zn in this system (only 30% of the total ^{1}Zn is, in fact, detected in this experiment), can be assigned to a minor impurity. [f] Aggregation phenomena can be responsible for nonexponential decay in polar solvents at 77 K.[27] [g] Weak emission.

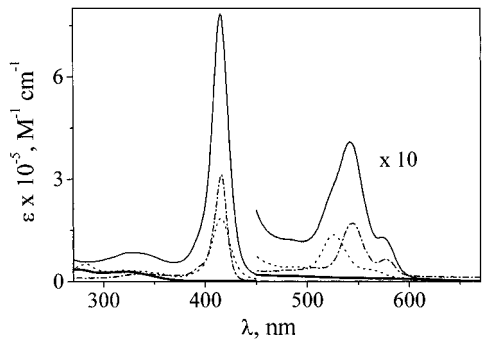

Figure 7. Absorption spectra of $\mathbf{Zn_2Cu}^+\mathbf{Au}^+$ (—), **Zn** (•—•), $\mathbf{Au}^+$ (•••) and $\mathbf{Cu}^+$ (▬) in acetonitrile, 298 K.

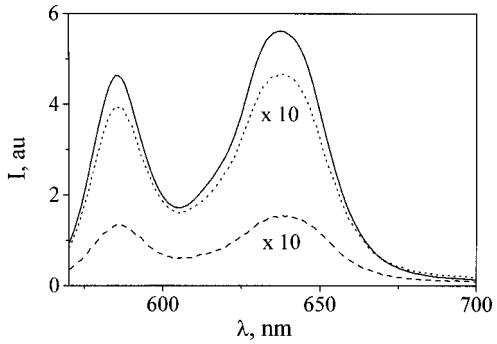

Figure 8. Fluorescence spectra of (—) **Zn**, $A = 0.16$; (- - -) $\mathbf{Zn_2}$–$\mathbf{Au}^+$, $A = 0.18$; and (•••) $\mathbf{Zn_2Cu}^+\mathbf{Au}^+$, $A = 0.19$ in acetonitrile solutions at 298 K upon excitation at 545 nm. The sample absorbances were adjusted to have the same number of photons absorbed by the Zn porphyrin moiety at the excitation wavelength.

Scheme 1

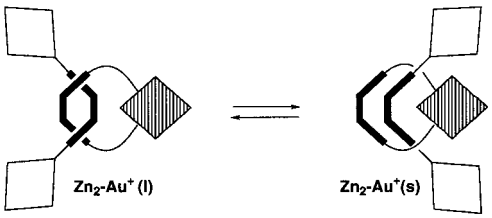

nm) for both rotaxanes and porphyrin models under comparable conditions[32] and are displayed in Figure 9. Representative

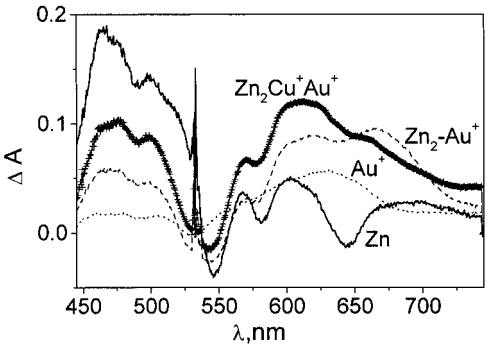

Figure 9. Differential transient absorbance at the end of a 35-ps pulse (532 nm, 2.5 mJ) in acetonitrile solutions for (•••) $\mathbf{Au}^+$, $A = 0.11$; (- -) $\mathbf{Zn_2}$–$\mathbf{Au}^+$, $A = 0.41$; (+) $\mathbf{Zn_2Cu}^+\mathbf{Au}^+$, $A = 0.43$; and (—) **Zn**, $A = 0.21$. The sample absorbances were adjusted to have the same number of photons absorbed by the Zn and Au porphyrin moieties at the excitation wavelength.[32] To achieve dissolution of **Zn**, butyronitrile was added, up to 70%.

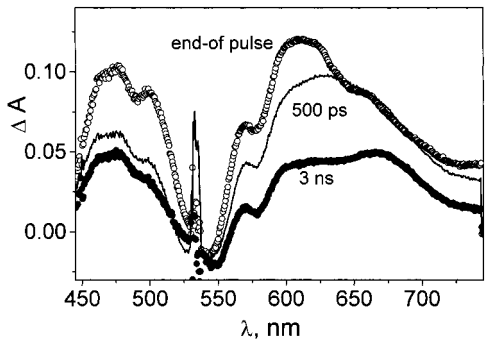

Figure 10. Differential transient absorbance of a $\mathbf{Zn_2Cu}^+\mathbf{Au}^+$ solution ($A = 0.43$) in acetonitrile after a 35-ps laser pulse (532 nm, 2.5 mJ). (○) End of pulse; (—) 500 ps; and (●) 3 ns.

wavelengths are 466 nm for ^{1}Zn; 616 nm for ^{3}Au$^+$, with some contribution of Au•,[33] and 670 nm for Zn$^{+\bullet}$.[34]

In Figure 10 are reported the spectra obtained for $\mathbf{Zn_2Cu}^+$-$\mathbf{Au}^+$ at the end of the laser pulse, and with delays of 500 ps and 3 ns. The initial spectrum shows the typical ^{1}Zn and ^{3}Au$^+$ features, the latter being present also in the 500-ps spectrum, with a prominent band around 630 nm, while the 3-ns spectrum has maxima at 610 and 670 nm and decays on the nanosecond time scale.

(32) At 532 nm, the partition of photons is 60% on zinc porphyrin, 37% on gold porphyrin and 3% on the Cu^+ unit for $\mathbf{Zn_2Cu}^+\mathbf{Au}^+$. For $\mathbf{Zn_2}$–$\mathbf{Au}^+$, 62% is on zinc porphyrin, and 38% is on gold porphyrin.

(33) Fajer, J.; Borg, D. C.; Forman, A.; Dolphin, D.; Felton, R. H. *J. Am. Chem. Soc.* **1970**, *92*, 3451−3459.

(34) Abou-Gamra, Z.; Harriman, A.; Neta, P. *J. Chem. Soc., Faraday Trans. 2*, **1986**, *82*, 2337−2350.

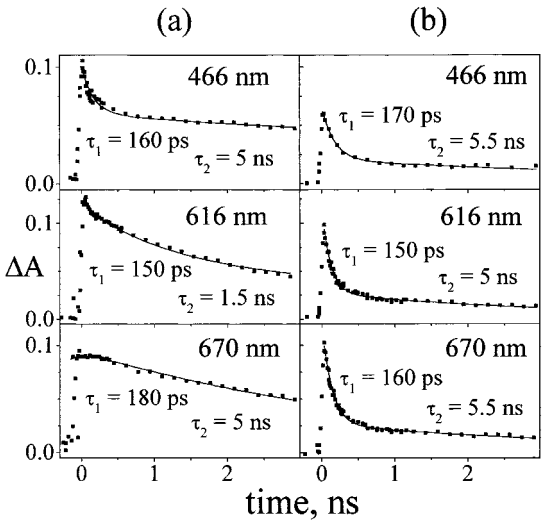

Figure 11. Transient absorbance decays and fittings for 466, 616, and 670 nm for $\mathbf{Zn_2Cu^+Au^+}$ (a) and $\mathbf{Zn_2{-}Au^+}$ (b). The conditions are the same as for Figures 10 and 13.

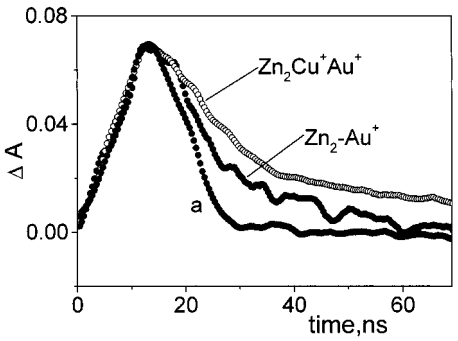

Figure 12. Normalized transient absorbance signal (average of 10 shots) detected after a 18-ns laser pulse (532 nm, 2 mJ) in acetonitrile solutions at $\lambda = 670$ nm for $\mathbf{Zn_2Cu^+Au^+}$ and $\mathbf{Zn_2{-}Au^+}$. Curve a is the instrumental response function.

The kinetic traces at the three representative wavelengths above are reported in Figure 11a. The decays at 466 and 670 nm can be fitted by the same exponentials, ca. 170 ps and 5 ns. However, at 670 nm, the shorter component appears as a formation, that is, with a negative preexponential factor. The 616 nm decay, which also shows a fast component (150 ps), is dominated by a lifetime of 1.5 ns. On the basis of its spectral shape and lifetime, it is due to the gold porphyrin-localized triplet, which is directly formed by the 532-nm excitation.[32] The fast decay (ca. 150−180 ps), which is detected predominantly around 470 nm, can be assigned to the $\mathbf{{}^1Zn_2Cu^+Au^+}$ state and is in reasonable agreement with the fluorescence decay (180 ps). It is coincident with the rate of formation of $Zn^{\bullet+}$ (670 nm), which then decays with a lifetime on the order of nanoseconds. The band with a maximum around 610 nm ($Au^{\bullet}$) also decays within the same time window. Therefore, we assign the 3-ns spectrum reported in Figure 10 to the fully charge-separated state (CS) $\mathbf{{}^{+\bullet}Zn_2Cu^+Au^{\bullet}}$. Its decay (ca. 5 ns) is shown in Figure 12 on a longer time scale. The residual absorbance after the CS state decay in Figure 12 is due to the $\mathbf{{}^3Zn_2Cu^+{-}Au^+}$ state, the Zn porphyrin-localized excited triplet (Table 5).

In Figure 13 are reported the spectra recorded for $\mathbf{Zn_2{-}Au^+}$ immediately and with delays of 190 ps, 530 ps, and 3 ns after the laser pulse. These spectra are characterized by prominent bands at 610 and 670 nm from the very beginning and, in contrast to the previous case, there is apparently no remarkable spectral change in the time evolution; the spectrum at 3 ns is very similar to the initial spectrum and to the one obtained at the same delay in the case of $\mathbf{Zn_2Cu^+Au^+}$ (Figure 10). Therefore, it is assigned to the charge-separated state $\mathbf{{}^{+\bullet}Zn_2{-}Au^{\bullet}}$. As shown in Figure 12, no residual absorption due to the Zn porphyrin-localized triplet can be detected after the CS state has disappeared. The decays of the transient absorbances at the three representative wavelengths defined above are reported in Figure 11b. In all three cases, the overall decay can be fitted by a double exponential function with lifetimes of 160 ps and 5.5 ns. If one assumes similar absorption coefficients for the two CS states $\mathbf{{}^{+\bullet}Zn_2{-}Au^{\bullet}}$ and $\mathbf{{}^{+\bullet}Zn_2Cu^+Au^{\bullet}}$, comparison of Figures 11a and 11b at sufficiently long delay indicates for $\mathbf{{}^{+\bullet}Zn_2{-}Au^{\bullet}}$ a yield which is ca. 30% of that of $\mathbf{{}^{+\bullet}Zn_2Cu^+Au^{\bullet}}$. This strongly suggests that in the free rotaxane the long-lived CS state is formed in the extended conformer $\mathbf{Zn_2{-}Au^+(l)}$ only.

Charge separation in the other conformer $\mathbf{[Zn_2{-}Au^+(s)]}$ is much faster. The shape of the initial transient absorption spectra of $\mathbf{Zn_2{-}Au^+}$ can be explained by the fast reactivity of the excited states $\mathbf{{}^1Zn_2{-}Au^+(s)}$ and $\mathbf{Zn_2{-}{}^3Au^+(s)}$ and by the minor contribution of the states derived from the $\mathbf{Zn_2{-}Au^+(l)}$ conformation because of its lower population (30%). Consequently, the typical $^3Au^+$ band around 620−630 nm is not so evident as in the case of $\mathbf{Zn_2Cu^+Au^+}$. The lifetime (160 ps) of the fast component suggests that it could be assigned to the decay of $\mathbf{{}^1Zn_2{-}Au^+(l)}$. However, because the end-of-pulse absorbance is higher than expected from the $\mathbf{{}^1Zn_2{-}Au^+(l)}$ state only, the existence of an underlying absorption of comparable lifetime, ascribable to the charge-separated state $\mathbf{{}^{+\bullet}Zn_2{-}Au^{\bullet}(s)}$ must be considered. Therefore, at least for the initial stages of the time evolution, some contribution of the transients derived from

Table 5. Transient Absorbance Data[a]

	state	τ (ns)	ϕ
Zn[b]	^{3}Zn	8 000	0.95[c]
$\mathbf{Au^+}$	$^3Au^+$	1.5	1[d]
$\mathbf{Cu^+}$	$^3Cu^+$	179[e]	
$\mathbf{Zn_2{-}Au^+}$	^{1}Zn	0.160	
	^{3}Zn		< 0.05[c]
	$^3Au^+$	n.d.	n.d.
	$^{\bullet+}$Zn−Au$^{\bullet}$	5.5	0.3[f]
$\mathbf{Zn_2Cu^+Au^+}$	^{1}Zn	0.170	
	^{3}Zn	1700	0.13[c]
	$^3Au^+$	1.5	1[c]
	$^{\bullet+}$ZnCu$^+$Au$^{\bullet}$	5	1[f]

[a] Oxygen-free acetonitrile for $\tau > 10$ ns. [b] Oxygen-free acetonitrile/butyronitrile (1/1). [c] Triplet-state quantum yields. For the rotaxanes, these are calculated on the basis of the photons absorbed by Zn or Au^+ porphyrin moiety only. [d] Assumed to be identical to that of the gold (III) tetraphenylporphyrin.[5b] [e] In deaerated CH_2Cl_2.[30] [f] Relative yield (see text).

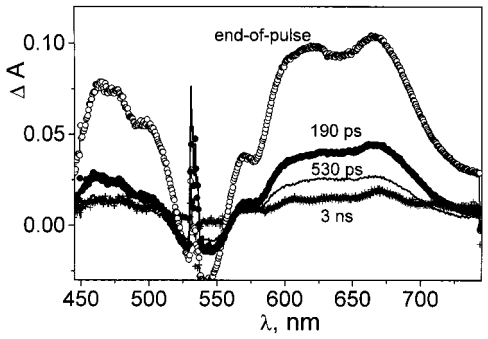

Figure 13. Differential transient absorbance of a $\mathbf{Zn_2{-}Au^+}$ solution ($A = 0.41$) in acetonitrile after a 35-ps laser pulse (532 nm, 2.5 mJ). (○) End of pulse spectrum; (●) 190 ps; (−) 530 ps; and (+)3 ns.

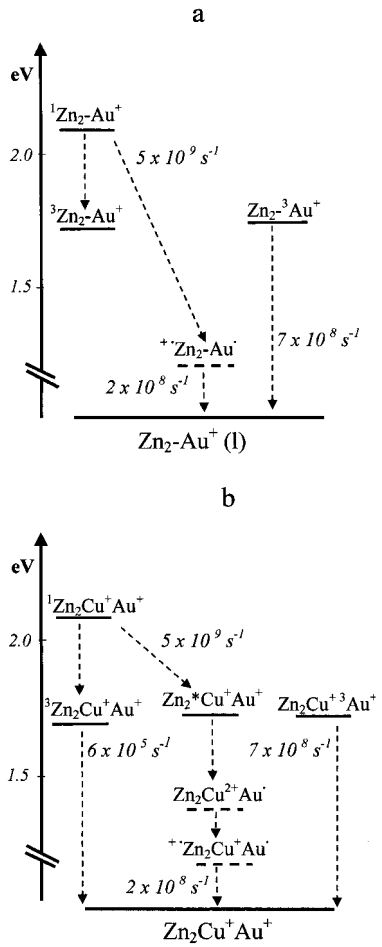

Figure 14. Schematic energy levels diagrams for **Zn$_2$**−**Au$^+$** (a) and **Zn$_2$Cu$^+$Au$^+$** (b). For the case of **Zn$_2$**−**Au$^+$**, only the rate parameters of the **Zn$_2$**−**Au$^+$(l)** conformation are reported.

Zn$_2$−**Au$^+$(s)**, in particular those due to the CS state $^{+\bullet}$**Zn$_2$**−**Au$^{\bullet}$(s)**, can be envisaged.

5. Photoinduced Electron Transfer. The energy level diagrams of **Zn$_2$**−**Au$^+$** and **Zn$_2$Cu$^+$Au$^+$**, using the data of Tables 2 and 4, are reported in Figure 14. They differ by the presence, in the case of **Zn$_2$Cu$^+$Au$^+$**, of a MLCT[35,36] excited state localized at the copper complex fragment (**Zn$_2$*Cu$^+$Au$^+$**), and the presence of a low-lying additional charge-separated state, **Zn$_2$Cu^{2+}Au$^{\bullet}$**. This CS state is 0.2 eV higher in energy than the fully CS state $^{+\bullet}$**Zn$_2$Cu$^+$Au$^{\bullet}$**. Within the weak interaction limit, the rates of the observed intramolecular processes can be calculated according to eq 1.

$$k = 1/\tau - 1/\tau_0 \qquad (1)$$

τ and τ_0 are the lifetimes of the chromophore unit in the rotaxanes and in the model, respectively. Photoinduced processes will be discussed in the frame of current theories of energy[37] and electron transfer.[38]

For **Zn$_2$**−**Au$^+$**, the processes can be clearly resolved only in the case of the extended conformation **Zn$_2$**−**Au$^+$(l)**. In the case of the **Zn$_2$**−**Au$^+$(s)** conformer, they can not be resolved because they are faster than the time resolution available (20 ps). Upon excitation of the zinc porphyrin subunit, **^{1}Zn$_2$**−**Au$^+$(l)** is formed, followed by electron transfer to the gold porphyrin ($\Delta G = -0.9$ eV), with a rate of 5.3×10^9 s^{-1}. Energy transfer to form **Zn$_2$**−**^{3}Au$^+$(l)** is forbidden for spin multiplicity. Electronic communication between the mechanically linked chromophores is likely provided by van der Waals interactions between the axle and the wheel of the rotaxane, as has been observed in donor−acceptor systems connected by hydrogen bonds[39] or in similarly mechanically linked species.[40] The yield of **^{3}Zn$_2$**−**Au$^+$**, the lowest-energy excited state of the system, is near zero. This indicates that energy transfer processes are not operative in **Zn$_2$**−**Au$^+$(l)**, which supports the electron transfer interpretation.

In the case of **Zn$_2$Cu$^+$Au$^+$**, sensitization of the **Zn$_2$*Cu$^+$**-**Au$^+$** state by energy transfer from the zinc porphyrin-localized singlet excited state (**^{1}Zn$_2$Cu$^+$Au$^+$**) is likely to occur at first. The mixed-singlet and -triplet nature of the emitting MLCT state of the Cu(I) bis-phenanthroline complexes[35,36] makes this energy transfer process allowed by spin selection rules. In addition, the quenching rate of **^{1}Zn$_2$Cu$^+$Au$^+$** (5×10^9 s^{-1}) is identical to that observed in a related [3]-rotaxane, for which energy transfer between the same chromophores was proven unequivocally.[27] This process is followed by electron transfer to the nearby gold porphyrin ($\Delta G = -0.3$ eV) with formation of the **Zn$_2$Cu^{2+}Au$^{\bullet}$** CS state. Subsequently, fast charge shift from a zinc porphyrin unit ($\Delta G = -0.25$ eV), produces the lowest energy CS state, $^{+\bullet}$**Zn$_2$Cu$^+$Au$^{\bullet}$**. It was not possible to detect these consecutive electron-transfer steps within the 20 ps time resolution. Therefore, the energy transfer step is rate-determining in the CS process. Intersystem crossing of **^{1}Zn$_2$Cu$^+$Au$^+$** to **^{3}**-**Zn$_2$Cu$^+$Au$^+$** is now competitive, because the zinc porphyrin-localized triplet is formed with a yield close to 0.1.

The CS states $^{+\bullet}$**Zn$_2$Cu$^+$Au$^{\bullet}$** and $^{+\bullet}$**Zn$_2$**−**Au$^{\bullet}$** decay at a very similar rate (2×10^8 s^{-1}) to re-form the ground state upon charge recombination. This is rather surprising because electronic communication between the oxidized and the reduced porphyrins is expected to be very different in the two systems.[41]

This result could be rationalized from a different viewpoint. It was assumed and confirmed by the data that the **Zn$_2$**−**Au$^+$**-**(l)** and **Zn$_2$**−**Au$^+$(s)** conformations did not interconvert within the time-scale of forward electron transfer. The same assumption could not hold true for longer time scales during which the conformers would be exchanging. In this case, the lifetime of 5.5 ns, which was detected for the charge recombination reaction in **Zn$_2$**−**Au$^+$**, could in fact measure the rate of conversion of $^{+\bullet}$**Zn$_2$**−**Au$^{\bullet}$(l)** to $^{+\bullet}$**Zn$_2$**−**Au$^{\bullet}$(s)**.[42] The latter CS state would immediately return to the ground state because of the closer

(35) The spin multiplicity has been omitted in **Zn$_2$*Cu$^+$Au$^+$** (the MLCT excitedstate localized on the copper complex) to underline the mixed nature of the emitting state. According to current interpretation,[36] the emission originates from a ^{1}MLCT in equilibrium at room temperature with a ^{3}-MLCT excited state.

(36) Kirchhoff, J. R.; Gamache, R. E. Jr.; Blaskie, M. W.; Del Paggio, A. A.; Lengel, R. K.; McMillin, D. R. *Inorg. Chem.* **1983**, *22*, 2380−2384.

(37) (a) Dexter, D. L. *J. Chem. Phys.* **1953**, *21*, 836−850. (b) Förster, T. *Discuss. Faraday Soc.* **1959**, *27*, 7−17. (c) Closs, G. L.; Johnson, M. D.; Miller, J. R.; Piotrowiak, P. *J. Am. Chem. Soc.* **1989**, *111*, 3751−3753.

(38) (a) Marcus, R. A.; Sutin, N. *Biochim. Biophys. Acta* **1985**, *811*, 322−265 and references therein. (b) Closs, G. L.; Miller, J. R. *Science* **1988**, *240*, 440−447 and references therein. (c) Piotrowiak, P. *Chem. Soc. Rev.* **1999**, *28*, 143−150.

(39) (a) De Rege, P. J. F.; Williams, S. A.; Therien, M. J. *Science* **1995**, *269*, 1409−1413. (b) Roberts, J. A.; Kirby, J. P.; Nocera, D. G. *J. Am. Chem. Soc.* **1995**, *117*, 8051−8052. (c) Ward, M. D.; White, C. M.; Barigelletti, F.; Armaroli, N.; Calogero, G.; Flamigni, L. *Coord. Chem. Rev.* **1998**, *171*, 481−488.

(40) Hu, Y.-Z.; Bossmann, S. H.; Van Loyen, D.; Schwarz, O.; Durr, H. *Chem. Eur. J.* **1999**, *5*, 1267−1277.

(41) The rate of electron transfer, k_{el}, can be expressed[38a] as $k_{el} = \nu e^{-\Delta G\#/RT}$, where the preexponential is the so-called "electronic factor" and the exponential is generally referred to as the "nuclear factor". The latter factor is mainly affected by thermodynamic parameters, which is similar in the two rotaxanes. The electronic factor depends on the overlap between electronic wave functions of the partners, and the interposed connector is crucial in determining the degree of overlap.

(42) Deleuze, M. S.; Leigh, D. A.; Zerbetto, F. *J. Am. Chem. Soc.* **1999**, *121*, 2364−2379.

proximity of the oxidized/reduced chromophores. The rate-determining step of the charge recombination in $\mathbf{Zn_2}-\mathbf{Au}^+$ could therefore be the interconversion between conformers.

Conclusion.

A detailed comparison of the properties of the free and the Cu(I)-complexed rotaxanes showed that the role of the Cu complexation is important in different perspectives: (i) it gives a geometric constraint which keeps the reacting partners at a fixed distance; (ii) it connects from an electronic viewpoint the primary electron donor, one of the two zinc porphyrins, and the electron acceptor, the gold porphyrin; and (iii) it offers an energy transfer pathway by means of its MLCT excited state. The absence of the copper ion in the $\mathbf{Zn_2}-\mathbf{Au}^+$ rotaxane, on the contrary, gives origin to a loose structure for which the distance and the mutual orientation of the components can vary, giving origin to different conformers. From the electronic perspective, the potential donor and acceptor units in $\mathbf{Zn_2}-\mathbf{Au}^+$ are not connected by chemical bonds, and no alternative energy transfer pathway is offered to the deactivation of $^1\mathbf{Zn_2}-\mathbf{Au}^+$, in contrast to the case of $^1\mathbf{Zn_2Cu}^+\mathbf{Au}^+$ which can transfer energy to the MLCT excited-state localized on the copper complex.

Experimental Section

Spectroscopic and Photophysical Measurements. The solvent used was acetonitrile (C. Erba, spectroscopic grade). Addition of butyronitrile (Fluka) up to 50−70% was necessary to dissolve the porphyrin **Zn** at the desired concentrations. Absorption spectra were recorded using a Perkin-Elmer Lambda 9 spectrophotometer. Uncorrected emission spectra were detected by a Spex Fluorolog II spectrofluorimeter equipped with a Hamamatsu R-928 photomultiplier tube. The 77 K phosphorescence spectra of the porphyrin triplets were detected by the same spectrofluorimeter equipped with a phosphorimeter accessory (1934D, Spex). Parameters to detect ^{3}Zn phosphorescence were excitation at 550 nm and gate open for 70 ms, with 1 ms delay with respect to excitation. Parameters used to detect $^3Au^+$ phosphorescence were excitation at 525 nm and gate open for 200 μs, with a delay of 20 μs with respect to the excitation. Experiments at 77 K were performed on samples contained in quartz capillary tubes immersed in a homemade quartz dewar filled with liquid nitrogen. The fluorescence quantum yield of **Zn**, determined by the method of Demas and Crosby[43] using $[Ru(bpy)_3]Cl_2$ in aerated water as standard ($\Phi = 2.8 \times 10^{-2}$), was 0.01.

Nanosecond flash photolysis studies were performed using a Nd:YAG laser (532 nm, 1−2 mJ per pulse). Samples were deaerated by bubbling argon in home-modified quartz cuvettes. Optical densities of solutions of the arrays for this experiments were 0.4−1. Transient absorption spectra in the picosecond time domain were measured by a pump and probe system. The second harmonic (532 nm) of a Nd:YAG laser (Continuum PY62−10) with a 35-ps pulse was used to excite the samples with an energy of 2−3 mJ. Optical density of the samples at the excitation wavelength was kept between 0.1 and 0.5. Details on the nanosecond laser flash photolysis and the picosecond pump−probe system can be found elsewhere.[44]

The yield of ^{3}Zn was determined by a comparative method using zinc tetraphenylporphyrin in benzene as standard[45] ($\Phi_T = 0.81$; $\Delta\epsilon_{470} = 73\,000$ $M^{-1}cm^{-1}$); the singlet depletion method[46] was used to determine the $\Delta\epsilon_{470}$ of ^{3}Zn, 90 000 $M^{-1}cm^{-1}$. The yield of $^3Au^+$ was assumed to be identical to that of the gold(III) tetraphenylporphyrin.[28] Yields of formation of the porphyrin triplets (Φ_T) in the arrays were determined by comparing the transient absorbances at 620−650 nm, the wavelength region out of ground-state absorption, with the corresponding values of the model compounds **Zn** and $\mathbf{Au}^+$ and by making corrections for the fraction of light absorbed at 532 nm by the moiety of interest in the sample. It was assumed that the molar absorption coefficients of triplets were unaffected in passing from models to the arrays. For the determination of the yield of $\mathbf{Zn_2Cu}^{+3}\mathbf{Au}^+$, the absorbance at 620 nm at the end of the pulse was corrected for the contribution of the charge-separated state.

Emission lifetimes in the micro- to millisecond range were measured by using as the excitation source a Nd:YAG laser (20-ns pulse) and a Hamamatsu R936 photomultiplier tube as the detector. The light emitted was collected at a right angle with respect to the excitation (1−2 mJ at 532 nm), selected by a series of filters, then directly fed into the photomultiplier, which was coupled to a digital oscilloscope. A Hamamatsu C1587 streak camera was used as the detector for fluorescence lifetimes below 2.5 ns. In this case, the excitation source was the same Nd:YAG laser as was used for absorption ($\lambda = 532$ nm, ca. 1 mJ, 35-ps pulse). Time and spectral profiles were derived from the streak image, which resulted from the average of several hundred shots. The time profiles were analyzed by standard iterative methods according to a single or a double exponential fitting.

The energies of the electronic levels of the various compounds were derived from the maxima of the luminescence bands at 77 K. Experimental uncertainties are estimated to be within 8% for lifetime determination, 15% for quantum yields, 20% for molar absorption coefficients, and 3 nm for emission and absorption peaks. The working temperature was 298 K, unless otherwise stated.

Acknowledgment. We warmly thank Vincent Semetey for his initial contribution to the synthesis of compounds **2**−**4**, and **9** and MALDI-TOF mass spectrometry measurements. We are grateful to Jean-Daniel Sauer for the high-field NMR spectra, and Raymond Hueber for the FAB mass spectra. We thank M. Minghetti for technical assistance and A. Martelli for electronic support. M.L. thanks the French Ministry of Education, Research, and Technology for a fellowship. We thank the European Communities for support through TMR contracts FMRX-CT96-0031 (M.L.) and FMRX-CT98-0226 (S.E.). This research was funded by CNR (Italy) and CNRS (France).

Supporting Information Available: Preparation of compounds **2** − **6**, **9** − **11**, $[\mathbf{Au}^+](PF_6^-)$, $[\mathbf{Cu}^+\mathbf{Au}^+](PF_6^-)_2$, $[\mathbf{(H_2)_2Cu}^+\mathbf{Au}^+](PF_6^-)_2$, $[\mathbf{Zn_2Cu}^+\mathbf{Au}^+](PF_6^-)_2$, $[\mathbf{Zn_2}-\mathbf{Au}^+](PF_6^-)$, $[\mathbf{Zn_2Ag}^+\mathbf{Au}^+](PF_6^-)_2$, and $[\mathbf{Zn_2Li}^+\mathbf{Au}^+](PF_6^-)_2$; electrochemistry. This material is available free of charge via the Internet at http://pubs.acs.org.

JA002018F

(43) Demas, J. N.; Crosby, G. A. *J. Phys. Chem.* **1971**, *75*, 991−1024.

(44) (a) Flamigni, L. *J. Phys. Chem.* **1992**, *96*, 3331−3337. (b) Flamigni, L. *J. Chem. Soc., Faraday Trans.* **1994**, *90*, 2331−2336. (c) Flamigni, L.; Armaroli, N.; Barigelletti, F.; Balzani, V.; Collin, J.-P.; Dalbavie, J.-O.; Heitz, V.; Sauvage, J.-P. *J. Phys. Chem. B* **1997**, *101*, 5936−5943.

(45) Tanielian, C.; Wolff, C. *J. Phys. Chem.* **1995**, *99*, 9825−9830.

(46) Bensasson, R. V.; Land, E. J.; Truscott, T. G. *Flash Photolysis and Pulse Radiolysis*; Pergamon Press: Oxford, 1983; pp 11−14.